Dissecting cellular function of fibronectin in osteoarthritic cartilage

Hoolwerff, M. van

Chapter 3

High-impact *FN1* mutation decreases chondrogenic potential and affects cartilage deposition via decreased binding to collagen type II

Marcella van Hoolwerff[1†], Alejandro Rodríguez Ruiz[1†], Marga Bouma[2,3], H. Eka D. Suchiman[1], Roman I. Koning[4], Carolina R. Jost[4], Aat A. Mulder[4], Christian Freund[2,3], Farshid Guilak[5], Yolande F.M. Ramos[1], Ingrid Meulenbelt[1]

[1] Dept. of Biomedical Data Sciences, Section Molecular Epidemiology, Leiden University Medical Center, Leiden, The Netherlands.
[2] LUMC hiPSC Hotel, Leiden University Medical Center, Leiden, The Netherlands.
[3] Dept. of Anatomy and Embryology, Leiden University Medical Center, Leiden, The Netherlands.
[4] Section Electron Microscopy, Department of Cell and Chemical Biology, Leiden University Medical Center, Leiden, The Netherlands.
[5] Dept. of Orthopedic Surgery, Washington University and Shriners Hospitals for Children, St. Louis, USA.
[†] These authors contributed equally to this work.

Sci Adv. 2021 Nov 5;7(45):eabg8583
doi: 10.1126/sciadv.abg8583

Abstract

Osteoarthritis is the most prevalent joint disease worldwide, yet progress in development of effective disease-modifying treatments is slow because of lack of insight into the underlying disease pathways. Therefore, we aimed to identify the causal pathogenic mutation in an early-onset osteoarthritis family, followed by functional studies in human induced pluripotent stem cells (hiPSCs) in an in vitro organoid cartilage model. We demonstrated that the identified causal missense mutation in the gelatin-binding domain of the extracellular matrix protein fibronectin resulted in significant decreased binding capacity to collagen type II. Further analyses of formed hiPSC-derived neo-cartilage tissue highlighted that mutated fibronectin affected chondrogenic capacity and propensity to a procatabolic osteoarthritic state. Together, we demonstrate that binding of fibronectin to collagen type II is crucial for fibronectin downstream gene expression of chondrocytes. We advocate that effective treatment development should focus on restoring or maintaining proper binding between fibronectin and collagen type II.

Introduction

Osteoarthritis (OA) is an age-related, degenerative, heterogeneous disease of the articular joints, characterized by pathological changes of the articular cartilage, synovium, and subchondral bone [1]. Currently, OA is the most prevalent joint disease worldwide and affects more than 40 million people in Europe alone [2, 3]. Patients with OA suffer pain and stiffness in the articular joints, resulting in significant disability in everyday life [4]. Despite these detrimental consequences, to date, no effective treatment is available except pain relief medication and, in the final stage, joint replacement surgery. Lacking insight into underlying OA pathophysiology has considerably contributed to failures in disease modifying OA drug development.

For that matter, next generation exome sequencing has been highly successful in identifying likely causal mutations in patients with familial, more severe phenotypes [5] or Mendelian disorders [6]. Because of their strong effect, these mutations can provide direct clues to genotype-phenotype relations and are more actionable to express a particular disease state in experimental human in vitro tissue models. Since the pathways in which these genes operate are likely extrapolated to confer risk to common OA, these mutations are destined to elucidate OA-specific aspects of the disease. Using cells carrying high-impact mutations in tailored human in vitro tissue models may thus elucidate previously unknown, likely causal underlying pathways of OA [7, 8]. Moreover, human induced pluripotent stem cell (hiPSC) technology allows reprogramming of primary cells into a sustainable pluripotent cell source, which is subsequently used for the directed differentiation into specialized cells of interest [9]. Even more, because of novel advancements in genomic engineering with CRISPR/Cas9 technology, cells are now easily edited or modulated. As a result, the creation of isogenic lines can give insight in the functional characterization of genetic variation. Since OA-relevant cells, such as chondrocytes, are not readily available, the combination of hiPSCs and CRISPR/Cas9 holds immense potential for translational human OA disease modeling to uncover the role of high-impact mutations [8].

By applying a genome-wide linkage scan in seven extended early-onset (EO)-OA families without dysplasia, we previously identified significant linkage on chromosome 2q33.3, with one family (family 2) that substantially contributed to this linkage area [10]. However, Sanger sequencing of 20 positional candidate genes located in the confined linkage region of these seven families failed to definitively identify the causal mutation in these families. More recently, an exome sequencing dataset was established in these OA families, resulting in the successful identification of a high-impact mutation in one of the families [11]. By applying a pathogenic prioritization scheme to the exome sequencing dataset of family 2, we identified a previously unidentified mutation and used hiPSCs and CRISPR/Cas9 technology to develop an in vitro organoid cartilage model to functionally characterize the effects of the causal mutation in this family.

Materials and Methods

Experimental design

The objective of the current study was to identify a likely causal pathogenic mutation in an EO-OA family and underlying disease pathways by functional analyses of isogenic hiPSCs. Exome sequencing was applied to identify a pathogenic mutation, whereas linkage analysis was applied to confirm co-segregation of the mutation and the OA phenotype. To study underlying mechanisms, the mutation was introduced in hiPSCs using CRISPR/Cas9 genome engineering, after which they were used in an in vitro organoid cartilage model, followed by functional analyses. A solid-phase binding assay was performed to quantify binding capacity of mutant and wild-type fibronectin to collagen type II.

Study populations

EO-OA family members

Previously, we reported on an EO family with primary generalized OA without dysplasia (**Supplementary Figure 1**) [10, 12]. The proband was collected through a Rheumatology outpatient clinic; family members were recruited via the proband. The age of onset of OA was between 23 and 45 and the phenotype is characterized by progressive OA with symptoms at multiple joints simultaneously. Two family members reported OA-related complaints, however, no radiographic evidence was available to confirm the diagnosis. An overview of the phenotypes is shown in **Supplementary Table 1**. The study was approved by the medical ethical committee and written and informed consent was obtained from all participants.

Controls

Occurrence of the *FN1* missense mutation was tested in the general population by de novo genotyping in healthy participants and OA cases. Middle-aged partners (N=744) of the offspring of nonagenarian siblings from the Leiden Longevity Study (LLS) [13] were considered as controls for OA cases were named 'random controls'. OA cases included were selected from the Genetics Osteoarthritis And Progression (GARP) study (N = 177) [14], the Patients Prospectively Recruited in Knee and hip Arthroplasty (PAPRIKA) study (N = 1,137) [15], and the ongoing Research osteoArthritis and Articular Cartilage (RAAK) study (N = 153) [16]. For more details on ascertainment of RAAK study biospecimen see Ramos *et al.* [11]. Ethical permission for the described studies was obtained from the appropriate medical ethical committee under protocol numbers P08.239 and P19.013. Written informed consent was obtained from all participants.

Exome sequencing

Exome sequencing of an affected EO-OA family member was performed by Illumina HiSeq2000 technology (Bejing Genome Institute). The sequences were generated as 100 base pair paired-end reads, after enrichment of 44 MB exonic sequences by NimbleGen EZ

(Roche NimbleGen). Raw imaging files were processed by Illumina base calling software version 1.7 with default parameters. SOAPaligner/SOAP2.21 was used to align reads to the GRCh37 reference genome at the UCSC Genome Browser website (http://genome.ucsc.edu/). Approximately, 70% of bases originated from the targeted exome, resulting in a mean coverage of 55.7-fold for the proband. More than 83% of the targeted exons were covered more than 10 times. Single-nucleotide variants were subsequently called by the SOAPsnps. The variant-filtering scheme, which resulted in 122 pathogenic mutations, is shown in **Supplementary Table 2**.

Genotyping

Single-nucleotide polymorphisms were genotyped by mass spectrometry (MassARRAY system, Sequenom, San Diego, CA) using standard conditions as described by Meulenbelt *et al.* [17]. Variants werWWe genotyped across available EO-OA family members (see **Supplementary Table 3**), OA case studies (GARP, PAPRIKA, and RAAK study), and random controls (LLS).

hiPSC line and cell culture

The hiPSC line LUMC0004iCTRL10 ("LUMC0004" in this manuscript) was generated from skin fibroblasts of a male donor without known genetic diseases ("wild type") as described previously [18], and registered at the Human pluripotent stem cell registry. The generation of the hiPSC line was approved by the Leiden University Medical Center ethical committee under P13.080. The hiPSCs were maintained under standard conditions (37 °C, 5% CO_2) on Vitronectin-XF (Stemcell Technologies)-coated plates and refreshed daily with TeSR-E8 medium (Stemcell Technologies). Cells were passaged in aggregates using Gentle Cell Dissociation Reagent (Stemcell Technologies) upon reaching approximately 80% confluency.

Genome editing of hiPSCs and clonal isolation

hiPSCs were dissociated with Gentle Cell Dissociation Reagent (Stemcell Technologies) and 1 x 10^5 cells were transfected with the Alt-R Cas9 RNP complex and the single-stranded oligodeoxynucleotide (ssODN; both IDT) using the NEON transfection System (Invitrogen) at 1200V/30 ms/1 pulse (for guide RNA and ssODN sequence see **Supplementary Table 4**). Cells were plated in a Synthemax II-SC (Corning)-coated plate using TeSR-E8 supplemented with CloneR (Stemcell Technologies). After recovery, 1000 cells were plated in a Synthemax II-SC-coated 10 cm dish in TeSR-E8 supplemented with CloneR and refreshed daily. After ~14 days, single cell-derived hiPSC colonies were manually picked, and one half was used for DNA isolation with QuickExtract Solution (Lucigen). Positive clones were identified by polymerase chain reaction (PCR) screening of the region of interest, followed by successful digestion by restriction enzyme HincII (New England Biolabs), according to manufacturer's instructions. Primer sequences are shown in **Supplementary Table 5**. The introduced mutation was confirmed by Sanger sequencing, performed by the Leiden Genome Technology Center.

Characterization of gene-edited hiPSCs

In silico analysis with the Cas-OFFinder tool [19] was used to identify most likely sites for off-target mutations. When allowing two mismatches, one potential off-target was identified, which was sequenced as described above (for primer sequences see **Supplementary Table 5**). G-banding analysis was conducted at the Laboratory of Clinical Genetics Leiden according to standard procedures. A total of 18 metaphases were analyzed for one heterozygous clone and 20 metaphases for one homozygous clone.

hiPSC differentiation to induced chondroprogenitor cells

Generation of human induced chondroprogenitor cells (hiCPCs) was based on a protocol previously described [20], which was shown to produce similar neo-cartilage to that produced by human primary articular chondrocytes [21]. When hiPSCs reached 60% confluence, the culture medium was switched to mesodermal differentiation (MD) medium, composed of IMDM GlutaMAX (IMDM; Thermofisher Scientific) and Ham's F12 Nutrient Mix (F12; Sigma-Aldrich) with 1% chemically defined lipid concentrate (Gibco), 1% insulin/human transferrin/selenous (ITS+; Corning), 0.5% penicillin/streptomycin (P/S; Gibco), and 450 μM 1-thioglycerol (Sigma-Aldrich). Before induction of anterior primitive streak (day 0) hiPSCs were washed with wash medium (IMDM/F12, 0.5% P/S) and then fed with MD medium supplemented with 30 ng/ml Activin A (Stemgent), 4 μM CHIR99021 (CHIR; Stemgent), and 20 ng/ml human fibroblast growth factor (FGF-2; R&D Systems) for 24 hours. Subsequently, the cells were washed again with wash medium and paraxial mesoderm was induced on day 1, by MD medium supplemented with 2 μM SB-505124 (Tocris), 3 μM CHIR, 20 ng/ml FGF-2, and 4 μM dorsomorphin (Tocris) for 24 hours. Before induction of early somite (day 2), cells were washed with wash medium, and then cells were fed with MD medium supplemented with 2 μM SB-505124, 4 μM dorsomorphin, 1 μM C59 (Cellagen Technology), and 500 nM PD173074 (Tocris) for 24 hours. Subsequently, cells were washed with wash medium, and for induction of sclerotome, cells (day 3-5) were fed daily with MD medium supplemented with 2 μM puromorphamine (Stemgent), and 1 μM C59. To induce chondroprogenitor cells (day 6-14), cells were washed briefly with wash medium and fed daily with MD medium supplemented with 20 ng/ml human bone morphogenetic protein 4 (BMP-4; Miltenyibiotec). Five independent differentiations were done per clone.

Chondrogenic differentiation

Monolayer cultured hiCPC aggregates present at day 14 of the differentiation were washed with MD medium, manually picked, and centrifuged for 4 minutes at 1200 rpm. Cell aggregates were subsequently maintained in Dulbecco's modified Eagle's medium/F12 (Gibco), supplemented with 1% ITS+, 55 μM 2-mercaptoethanol (Gibco), 1% non-essential amino acids (NEAA, Gibco), 0.5% P/S, 50 μg/ml L-ascorbate-2-phosphate (Sigma-Aldrich), 40 μg/ml L-proline (Sigma-Aldrich), and 10 ng/ml transforming growth factor-β1 (Prepotech) for 35 days while

refreshing medium every 3 to 4 days. The remaining hiCPC aggregates in the well were pooled and lysed with 500 µl TRIzol reagent (Thermo Fisher Scientific) and stored at -80 °C until further processing.

Sulfated glycosaminoglycan measurement

Sulfated glycosaminoglycan (sGAG) concentration in the chondrogenic pellets was measured with the 1,9-dimethylmethylene blue (DMMB) assay [22]. Pellets were digested with papain from papaya (Sigma-Aldrich) at 60 °C overnight. Shark chondroitin sulfate (Sigma-Aldrich) was used as a reference standard. The absorbance was measured at 525 and 595 nm in a microplate reader (Spectramax iD3; Molecular Devices).

Histology and immunohistochemistry

Chondrogenic pellets were fixed in 4% formaldehyde overnight and stored in 70% ethanol at 4 °C. They were then embedded in paraffin and sectioned at 5 µm. After sectioning, slides were deparaffinized and rehydrated. Overall cellular and tissue structure was visualized with hematoxylin and eosin staining. Sections were stained with 1% Alcian blue 8-GX (Sigma-Aldrich) and Nuclear Fast Red (Sigma-Aldrich) to visualize glycosaminoglycan deposition. To detect fibronectin (1:400; ab2413, Abcam), collagen type I (1:1000; ab34710, Abcam), and collagen type II (1:100; ab34712, Abcam), immunohistochemistry was performed with 3-diaminobenzidine solution (Sigma-Aldrich) and hematoxylin (Klinipath) as described before [23]. Alcian blue staining was quantified by loading the images in Fiji and splitting the color channels. Subsequently, grey values were measured of three to five separate squares per pellet and corrected for the grey value of the background.

RNA isolation and reverse transcription-quantitative PCR

For RNA isolation, two pellets were pooled and lysed in 200 µl of TRIzol reagent (Thermo Fisher Scientific) and homogenized using micro pestles. RNA was extracted with chloroform and purified from the supernatant using an RNeasy Mini kit (Qiagen). Synthesis of complementary DNA (cDNA) was performed with 150 ng of total RNA using a First Strand cDNA Synthesis kit according to manufacturer's protocol (Roche Applied Science). cDNA was diluted five times and preamplification with Taqman preamp master mix (Thermo Fisher Scientific) was performed for eight genes of interest. Primer sequences are shown in **Supplementary Table 5**. Gene expression was measured with the Fluidigm Biomark HD machine using a 96.96 IFC chip or with QuantStudio 6 Real-Time PCR system (Applied Biosystems) using FastStart SYBR Green Master reaction mix (Roche Applied Science). Quality control of the data was performed and non-detected values were removed. Relative gene expression levels were calculated with the $2^{-\Delta\Delta Ct}$ method as follows; the average of triplicate Ct values of the genes were averaged. Ct values of *GAPDH* and *SDHA* were averaged to function as reference genes (RG). Next, ΔCt values of the gene of interest (GOI) were calculated as $Ct_{GOI} - Ct_{RG}$.

Subsequently, we averaged the ΔCt values of *COL1A1* and *COL2A1* as chondrogenic controls (CC) to calculate final ΔCt values of the gene of interest, as followed: $\Delta Ct_{GOI\ new} = \Delta Ct_{GOI} - \Delta Ct_{CC}$. Fold changes were calculated with $2^{-\Delta\Delta Ct}$, with the wild type as reference.

Solid-phase binding assay

Conditioned medium of wild-type and *FN1* mutant pellets was collected and concentrated in preparation for the binding assay. To this end, 450 µl medium was collected in 100 K molecular weight cut-off Pierce Protein Concentrators (Thermo Scientific) and centrifuged for 10 min at 12,000 *g*. Subsequently, fibronectin concentration was determined using the Human Fibronectin enzyme-linked immunosorbent assay (ELISA) kit (Invitrogen) according to manufacturer's protocol.

Clear multiwell plates (R&D Systems) were coated overnight with 100 µl of purified human collagen type II (10 µg/ml; Merck) in phosphate-buffered saline (PBS) at 4 °C, followed by four wash steps with wash buffer (0.05% Tween-20 in PBS). Nonspecific binding was blocked for 1 hour with 3% (w/v) bovine serum albumin (BSA) in PBS. After washing with wash buffer, the plates were incubated with 100 µl concentrated medium samples at 40 ng/ml FN1 concentration in assay buffer (0.05% Tween-20, 0.5% BSA in PBS) for 2 hours. Plates were then washed four times with wash buffer and incubated with rabbit anti-fibronectin biotin conjugated antibody (Rockland) at 0.2 µg/ml in assay buffer for 1 hour. Plates were washed, after which the plates were incubated with streptavidin-horseradish peroxidase (Thermo Scientific) at 0.1 µg/ml in assay buffer for 1 hour. After washing, color development was performed with 100 µl tetramethyl-benzidine substrate (Thermo Fisher) for 10 min, reaction was stopped with 100 µl 1 M HCl and absorbance was measured at 450 nm. Assays were performed in triplicate. Error bars are SDs.

Transmission electron microscopy

Chondrogenic pellets that where embedded in paraffin were melted from the paraffin for 30 minutes at 62 °C. Subsequently, the samples were deparaffinized and rehydrated with a series of ethanol. The rehydrated samples were fixed again in 1.5% glutaraldehyde/0.1 M cacodylate buffer and after three times rinsing with 0.1 M cacodylate buffer, postfixed in 1% OsO4/0.1 M cacodylate buffer. A dehydration with a series of ethanol and series of propylene oxide mixed with EPON (LX112, Ladd research industries) was performed. After a final step with EPON the samples were each placed in a BEEM capsule; these were filled with EPON and polymerized at 70°C for 48 hours. Ultrathin sections (90 nm) were made on a Reichert Ultracut S (Leica Microsystems). After the poststaining of the sections with uranyl acetate and lead citrate, the electron microscopy images were taken with a twin transmission electron microscope (Thermo Fisher Scientific, formerly Fei) operating at 120 kV, using a Gatan Oneview camera (Gatan, Pleasanton) on binning 2. Overlapping images were collected and stitched together into a big image as previously described [24].

Statistical analysis

Statistical analyses were performed using SPSS version 25 (IBM). Data are shown as mean ± SD. With respect to reverse transcription-quantitative PCR (RT-qPCR) gene expression data, individual -ΔCt values are shown, as well as box plots per genotype. The box plots represent 25th, 50th and 75th percentiles, and whiskers represent the lowest and largest data point lying within 1.5 times the interquartile range. Individual samples are depicted by dots in each graph. The reported P values were determined by applying a generalized estimating equations (GEE) to the experimental readout i.e. -ΔCt values, relative Alcian blue intensity, and FN1 concentration, to effectively adjust for dependencies of the independent differentiations per genotype. In general we followed a linear GEE model, with the readout data as dependent variable, genotype as factor, and exchangeable working matrix: Read-out ~ Genotype + (1| Differentiation). To determine a dose-response effect, we applied a GEE to the experimental read-out, i.e. absorbance, and sGAG/DNA, with the read-out as dependent variable, genotype as covariate, and exchangeable working matrix. For the analysis of the pellet morphology, we followed a binary logistic GEE model, with normal and not-normal pellets as readout, genotype as factor, and adjusted for independent differentiations. P values < 0.05 were considered statistically significant. * P < 0.05, ** P < 0.01, *** P < 0.005.

Results

Identification of heterozygous missense mutation in *FN1*

Whole-exome sequencing was applied to an affected individual of an EO generalized OA family (**Figure 1A, subject 10**) with an average age of onset at 37 years and without dysplasia (**Supplementary Table 1**). This resulted in the identification of 73,407 variants after quality control, after which a prioritization scheme was applied to identify pathogenic variants (**Supplementary Table 2**). Hence, intergenic variants, intron variants, synonymous variants, and tolerated missense variants as determined by PolyPhen or SIFT (Sorting Intolerant From Tolerant) were excluded, as well as variants present in dbSNP build 124 (including 1000 Genomes Pilot project data). In addition, variants were excluded that were previously detected by whole-genome sequencing projects, in-house (N = 221), and by means of the BBMRI-Genome of The Netherlands project (N = 473) [25]. As a consequence, the number of variants was reduced to 122 missense variants (**Supplementary Table 6**) that were predicted to have a functional impact on the gene.

Previously, our group showed strong linkage on 2q33.3 with seven extended EO-OA families, including the family described in this study [10]. This family showed substantial contribution to this linkage area (logarithm of odds score 2.93); hence, we investigated the chromosomal location of the previously mentioned 122 missense variants. Of these variants, three were located around the linkage area on chromosome 2, namely, *ALS2*, *FN1*, and *ABCB6*. To explore

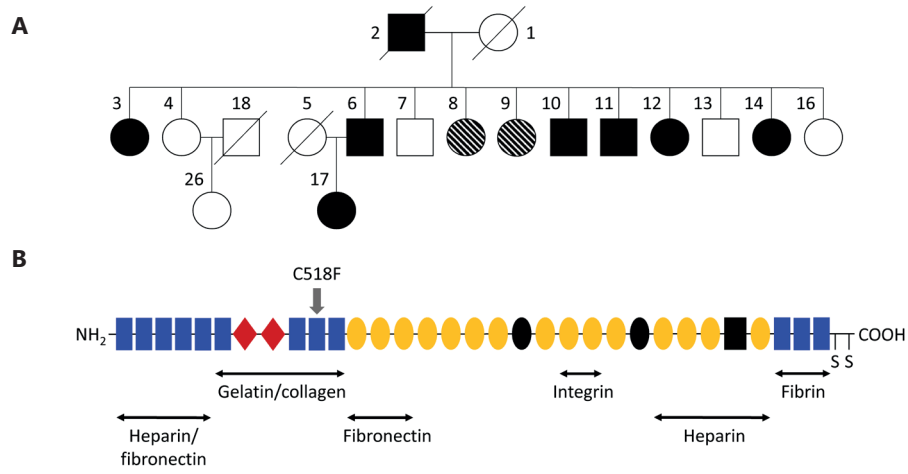

Figure 1 | High-impact mutation identified in *FN1* in early-onset osteoarthritis family. (**A**) Pedigree of investigated early-onset osteoarthritis family. Individual 10 was used for exome sequencing. Circles represent females, squares represent males. Closed and open shapes represent affected and healthy individuals, respectively, and striped shapes represent uncertain phenotypes, i.e., some complaints, but not confirmed by radiography. The diagonal line indicates deceased status. (**B**) Schematic diagram of a fibronectin subunit. Fibronectin consists of three types of repeats: type I (rectangle), type II (diamond), and type III (sphere). The C-terminal cysteines are involved in dimerization. The alternatively spliced sites are black shapes. Main binding sites for heparin, collagen, fibronectin and integrin are shown. Position of the identified C518F mutation is indicated by the grey arrow.

functionality of these genes in OA-relevant tissue, gene expression levels in our previously published RNA sequencing data of lesioned and preserved cartilage and bone samples of patients undergoing joint replacement surgery due to end-stage OA, from the RAAK study, were examined [26, 27]. *FN1* showed the highest gene expression in both cartilage and bone samples and showed a high, significant up-regulation (fold change, 2.12; false discovery rate = 1.17×10^{-3}) in lesioned compared with preserved OA cartilage (**Table 1**). Furthermore, *ALS2* was expressed at low levels in both cartilage and bone samples, while *ABCB6* expression was even lower in cartilage and not detected in bone. Therefore, de novo genotyping was performed for the *ALS2* and *FN1* variant, showing that the *ALS2* variant was not detected, yet confirming that the *FN1* variant was carried in seven affected individuals, but not in six unaffected family

Table 1 | Reproduced gene expression analysis of detected previously unidentified variants located around linkage area 2q33.3 in osteoarthritic cartilage and bone.

					Cartilage†			Bone†		
Position	**Gene**	**Codon**	**AA sub.**	**Base**	**Quartile**	**FC**	**FDR**	**Quartile**	**FC**	**FDR**
202590176	*ALS2*	TAT-gAT	Y1084D	A/C	Q3	1.1	4.95×10^{-1}	Q3	1.0	8.14×10^{-1}
216285518	*FN1*	TGC-TtC	C518F	C/A	Q4	2.1	1.17×10^{-3}	Q4	1.2	6.04×10^{-1}
220075737	*ABCB6*	CGT-gGT	R688G	G/C	Q1	1.1	8.72×10^{-1}	ND	ND	ND

AA sub.* = amino acid substitution; Base = base change; FC = fold change; FDR = false discovery rate of differential expression; ND = not detected. * Variants are novel, missense damaging, nonsense, readthrough, frame error or splice-sites not present in dbSNPv124, as well as not detected in in-house genome sequencing projects (LLS, N = 221) and analyzed human genomes by means of the Genome of The Netherlands (N = 473)[25]. † Expression levels in quartiles, with Q1 being the lowest and Q4 being the highest, fold changes and false discovery rate of differential expression levels of identified variants reproduced from RNA sequencing dataset of articular cartilage [26] and subchondral bone [27].

members. These data indicate complete linkage to robustly affected and unaffected subjects in the family (**Supplementary Table 3**). The *FN1* variant was neither present in the additional 1467 OA cases (GARP, RAAK, and PAPRIKA study) and 744 random controls (LLS), nor in the Genome Aggregation Database (version 2.1.1), and is therefore likely specific for this EO-OA family. Taken together, these data indicate that the G-to-T nucleotide change (c1,819), resulting in an amino acid change from cysteine to phenylalanine (C518F; **Figure 1B**) in the *FN1* gene is likely causal to the EO phenotype in this family.

FN1 encodes fibronectin, which is a dimeric glycoprotein, highly abundant in the extracellular matrix (ECM) of articular cartilage and more specifically localized in the pericellular matrix surrounding the chondrocyte. Fibronectin can bind to matrix proteins by multiple binding domains, such as the gelatin-binding domain which binds to collagen type II, as well as to cell surface integrins, thereby functioning as an adhesion molecule facilitating signals from the extracellular matrix to chondrocytes [28, 29]. Next, we aimed to investigate the molecular implications of the identified *FN1* mutation for the pathophysiology of OA.

Targeted gene editing of *FN1* mutation using CRISPR/Cas9 in hiPSCs

To elucidate the potential pathogenic mechanism of the identified *FN1* mutation, we sought to introduce it into wild-type hiPSCs, resulting in an isogenic pair of mutated and non-targeted hiPSCs. Gene editing was achieved by using CRISPR/Cas9, a guide RNA binding in close to proximity to the target site, as well as a 141-mer ssODN containing the specific *FN1* mutation (**Supplementary Table 4**). The creation of a HincII target site by introducing the mutation was used for screening of successfully targeted clones (**Figure 2A**). The presence of the introduced mutation was confirmed by Sanger sequencing (**Figure 2B**). A total of 274 hiPSC clones were screened, of which 14 (5.1%) were heterozygous and 3 (1.1%) were homozygous for the *FN1* mutation. Last, one heterozygous and one homozygous *FN1* mutant clone were selected for further experiments. Both clones had a normal karyotype, and the predicted off-target site allowing two mismatches was not altered (**Supplementary Figure 2**).

Effect of missense mutation *FN1* on chondrogenesis

The wild-type, heterozygous and homozygous *FN1* hiPSC clones were differentiated stepwise to the mesodermal lineage and further towards hiCPCs. Subsequently, hiCPC aggregates were manually picked, and chondrogenesis was initiated in our organoid cartilage model. After 5 weeks of chondrogenesis, the chondrogenic pellets were collected, where we observed different morphologies of the pellets. We categorized the pellets in groups based on shape (round or protrusive) and opaqueness of the matrix (**Figure 3A**). The abundance of round, dense pellets (**Figure 3A, group 1**) was 53% of the pellets in the wild-type group, while this decreased substantially to 15% in the heterozygous group, and to 18% in the homozygous group (**Figure 3B**). Furthermore, the abundance of protrusive pellets with more transparent

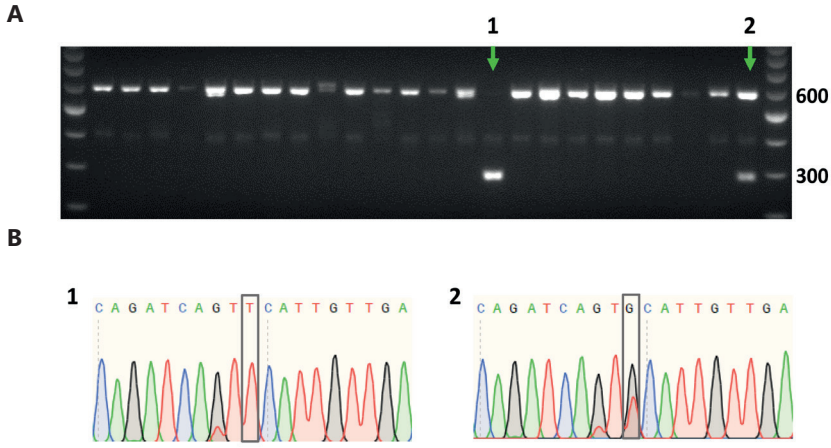

Figure 2 | Introducing identified *FN1* mutation in human induced pluripotent stem cells (hiPSCs). Clonal screen for *FN1* mutation in hiPSCs by genomic povlymerase chain reaction (PCR) followed by HincII digestion (**A**), confirmed by Sanger sequencing (**B**). The PCR product is 600 base pairs (bp) in size. Upon integration of the provided single-stranded oligodeoxynucleotide, HincII digestion results in 303- and 297-bp products. (**A**) Representative gel image, where *FN1* mutant clones are indicated by a green arrow, showing a homozygous clone (lane 1) and a heterozygous clone (lane 2). (**B**) Sanger sequencing results of homozygous (1) and heterozygous (2) clone, respectively. Grey box represents *FN1* mutation.

matrix (**Figure 3A, group 3**) in the heterozygous (60%), and homozygous (54%) groups was increased compared to the wild-type group (25%). When considering group 1 as 'normal' pellets and groups 2-4 as 'not-normal' pellets, we found a significant association between the occurrence of not-normal pellets and the presence of the *FN1* mutation, for both the heterozygous group (Beta = 1.84, 95% CI 2.8 – 14.1, P value = 9×10^{-6}) and the homozygous group (Beta = 1.63, 95% CI 2.4 – 11.1, P value = 3.1×10^{-5}). These data show that there is a dominant effect of the mutation on the formation of dense, round pellets, thus indicating an inhibited chondrogenic potential of the mutant hiCPCs.

To investigate whether the chondrogenic potential of the mutant hiCPCs was also inhibited before the chondrogenesis, we measured expression of the previously identified chondroprogenitor and chondrogenic markers *MCAM, PDGFRβ,* and *COL2A1* of hiCPCs at day 0 of chondrogenesis (**Figure 3C**) [20, 30-32]. *MCAM* was not differentially expressed between the groups, yet *PDGFRβ* and *COL2A1* expression was significantly down-regulated in the homozygous group, compared with wild type. Together, these data show that the chondrogenic potential is decreased as a result of the *FN1* mutation, with the effect being the most pronounced in the homozygous hiCPCs.

To characterize the differences between the normal and the not-normal chondrogenic pellets, we performed histological and immunohistochemical analyses (**Figure 4A**). Hematoxylin and eosin staining of chondrogenic pellets from group 3 showed that there was a clear difference

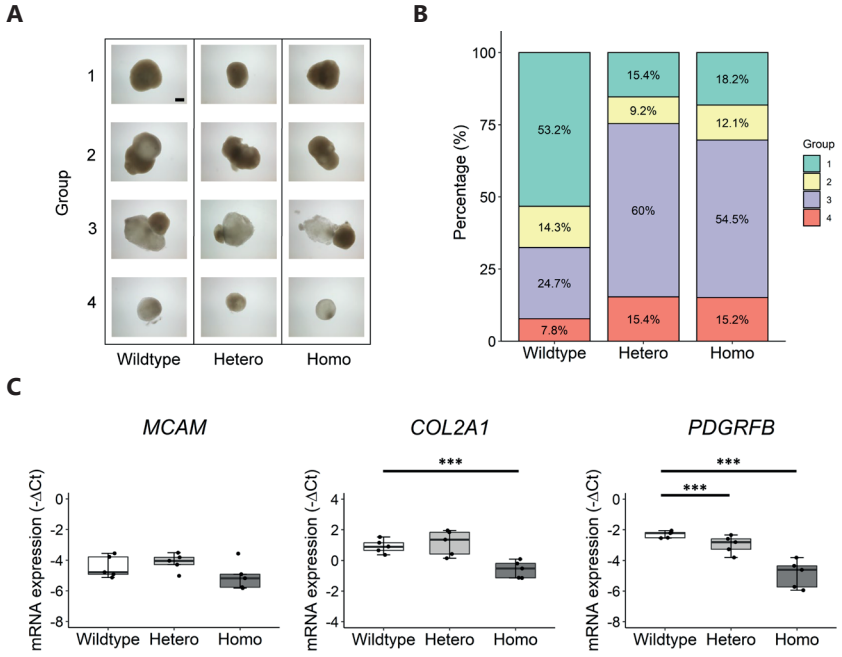

Figure 3 | Decreased chondrogenic potential of human induced chondroprogenitor cells (hiCPCs) as a result of the *FN1* mutation. (**A**) Representative images of the observed morphology of wild-type, *FN1* C518F heterozygous (Hetero), and C518F homozygous (Homo) hiCPC-derived chondrogenic pellets after 5 weeks of chondrogenesis in five independent differentiations. Pellets were categorized in four groups based on shape and opaqueness of the matrix: (1) Round and dense, (2) Protrusive and dense, (3) Protrusive and transparent, (4) Round and transparent. Scale bar, 400 μm. (**B**) Distribution of pellets in groups 1 to 4 of wild-type (N=77), *FN1* heterozygous (N=65), and *FN1* homozygous pellets (N=66). (N = 5-20 pellets per differentiation). (**C**) Gene expression levels depicted by -ΔCt values of hiCPC markers *MCAM*, *COL2A1*, and *PDGFRβ* [20] at day 0 of chondrogenesis of pooled wild-type and *FN1* mutant hiCPCs (N=5). The box plots represent 25th, 50th and 75th percentiles, and whiskers extend up to 1.5 times the interquartile range. Individual samples are depicted by black dots in each graph. P values were determined by generalized estimation equations, with gene expression levels (-ΔCt) as dependent variable and genotype as factor. *** P < 0.001.

in structure and composition between the dense and transparent matrix. Moreover, Alcian blue, fibronectin, collagen type I and II staining revealed that the transparent matrix was non-cartilaginous tissue. When only considering normal pellets (group 1), visually there was not a clear difference in matrix intensity staining of collagen type II and fibronectin (**Figure 4B**). However, quantification of the Alcian blue staining in the chondrogenic parts of pellets from groups 1 to 3 revealed a significant decrease in intensity in the *FN1* mutant chondrogenic pellets (**Figure 4C**). Quantification of the neo-cartilage sGAG deposition normalized to DNA content showed a significant linear reduction (Beta = -1.44, 95% CI 0.07 – 0.86, P = 2.8 x 10^{-2}) with the presence of the *FN1* mutation (**Figure 4D**). Moreover, fibronectin concentration was decreased in the medium of the *FN1* mutant pellets, albeit not significantly in the homozygous group (**Figure 4E**). Together, our data show that the *FN1* mutation results in a negative effect on chondrogenic potential and neo-cartilage deposition.

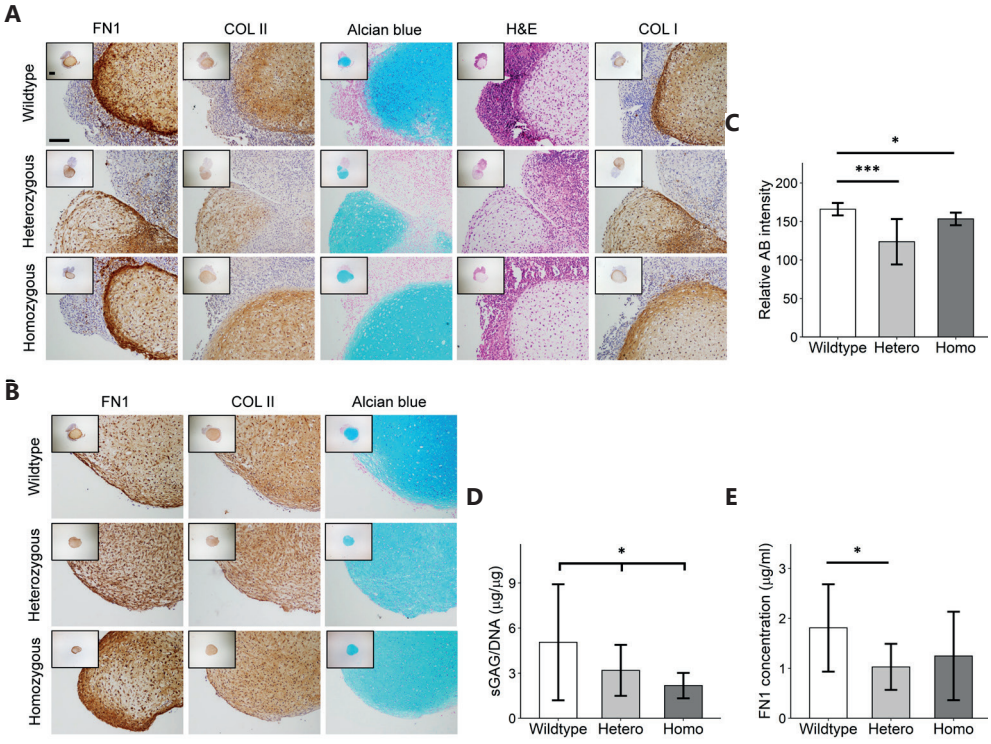

Figure 4 | Decreased neo-cartilage deposition in C518F *FN1* mutant chondrogenic pellets. (**A**) Representative images of wild-type and *FN1* mutant human induced chondroprogenitor cells (hiCPC)-derived chondrogenic pellets categorized in groups 2 to 4 analyzed by hematoxylin and eosin (H&E), Alcian blue, fibronectin (FN1), collagen type I (COL I), and collagen type II (COL II). Scale bar, 200 µm. (**B**) Representative images of wild-type and *FN1* mutant hiCPC-derived chondrogenic pellets categorized in group 1 analyzed by Alcian blue, fibronectin (FN1), and collagen type II (COL II). Scale bar, 200 µm. (**C**) Quantification of Alcian blue (AB) staining of Alcian blue-positive areas in wild-type and *FN1* mutant hiCPC-derived chondrogenic pellets (N=3). (**D**) Dose-response reduction (Beta = -1.44, P = 2.8 x 10^{-2}) of sulfated glycosaminoglycan (sGAG) normalized to DNA in wild-type, *FN1* heterozygous (Hetero) and homozygous (Homo) chondrogenic pellets analyzed by dimethylmethylene blue (N=8). (**E**) Fibronectin concentration in conditioned medium from *FN1* mutant pellets is decreased compared with wild-type, as determined by ELISA (N=3) . Data are means ± SD. P values were determined by generalized estimation equations, with experimental readout (relative Alcian Blue intensity, sGAG/DNA, and fibronectin concentration) as dependent variable and genotype as covariate (relative Alcian Blue intensity, sGAG/DNA) or factor (fibronectin concentration). * P < 0.05, *** P < 0.005.

Mechanism of reduced chondrogenesis in mutant chondrogenic pellets

The identified C518F mutation is located in the gelatin-binding domain of fibronectin, which is particularly involved in binding to collagen type II [29]. The cysteine is involved in intramolecular disulfide bond formation and was shown to be highly conserved among multiple species, highlighting the importance of this amino acid (**Supplementary Figure 3A**). The change from a polar cysteine to a nonpolar phenylalanine resulted in a predicted conformational change of the protein as determined by RaptorX [33] (**Supplementary**

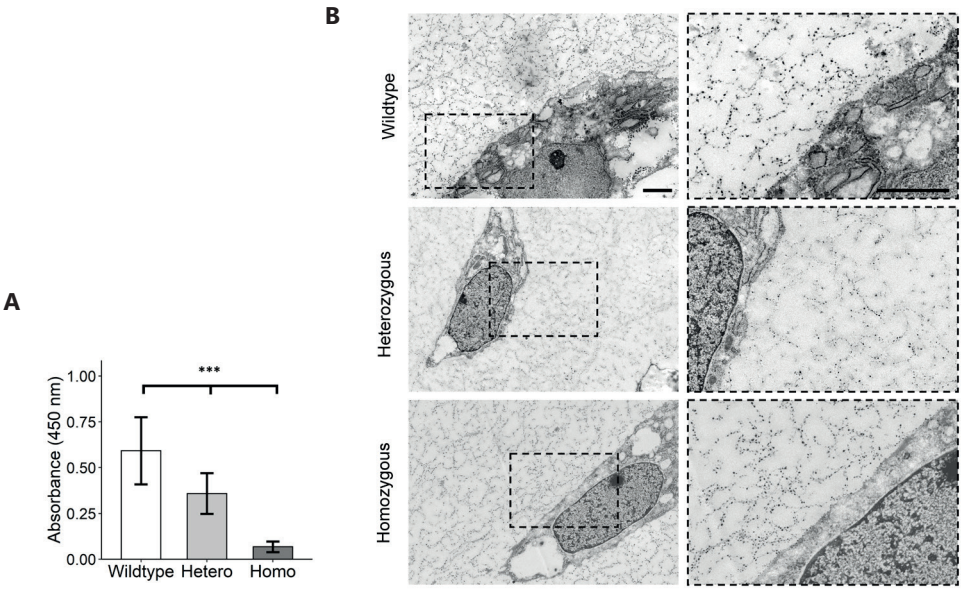

Figure 5 | *FN1* mutant fibronectin showed a dose-response decrease of binding capacity to collagen type II. (**A**) Solid-phase binding assay with collagen type II-coated wells and wild-type and C518F mutant fibronectin isolated from chondrogenic pellet cultures. Heterozygous (Hetero) and homozygous (Homo) mutant fibronectin showed linear reduction (Beta = -0.26 , P = 2.26 x 10^{-9}) of binding to collagen type II compared to wild-type fibronectin. Data are means ± SD (N = 3). P value was determined by generalized estimation equations, with absorbance as dependent variable and genotype as covariate. *** P < 0.005. (**B**) Representative transmission electron microscopy images showing a cell surrounded by cartilaginous matrix of wild-type and *FN1* mutant human induced chondroprogenitor cell-derived chondrogenic pellets. The fibrillar network surrounding the cells is suggestive of hyaluronic acid aggregates, and the dense particles are proteoglycans containing granules. Scale bars, 2 µm.

Figure 3B). When replaced by the phenylalanine, the disulfide bond in this part of the domain cannot be formed. Therefore we hypothesized that the mutation resulted in a conformational change in the gelatin-binding domain, with concurrent decreased binding of fibronectin to collagen type II. To explore this, we performed a collagen type II binding assay with wild-type, heterozygous, and homozygous mutant fibronectin. As a result, we observed a linear reduction (Beta = -0.26, 95% CI 0.71 – 0.84, P = 2.3x10^{-9}) in binding of mutant fibronectin to collagen type II relative to wild-type fibronectin, thereby confirming our hypothesis (**Figure 5A**). To further investigate whether we could identify structural differences in the neo-cartilage as a result of this decreased binding between fibronectin and collagen type II, we visualized cartilage by transmission electron microscopy. We observed electron dense particles that were present both attached to the plasma membrane and to a branching fibrillar network obviously devoid of striations emanating from the plasma membrane. The fibrillar network suggests a network of hyaluronic acid aggregates [34], and the electron dense particles are proteoglycans containing granules (**Figure 5B**) [35]. However, we could not identify any clear differences of the abundance and structure of observed structures between the wild-type and *FN1* mutant.

To study the effect of the mutation on markers reflecting chondrocytes in health or disease state, we next explored chondrocyte gene expression in the pellets as a result of the mutation by performing RT-qPCR for 10 relevant genes. Relative gene expression levels were first calculated by normalizing to expression levels of *GAPDH* and *SDHA* (**Supplementary Figure 4**). The observed difference in formation of neo-cartilage between the genotypes (**Figure 4A**) was potentially a confounding factor in the gene expression analysis. Therefore, we aimed to correct for the differences in efficiency of the neo-cartilage formation between the genotypes. Hence, we selected cartilage-specific markers that were highly expressed in our lesioned and preserved osteoarthritic cartilage samples (RAAK study), but without significant differential expression [26], and that we showed to be specific markers for the neo-cartilage (**Figure 4A**). As a result, *COL1A1* and *COL2A1* were selected as reference genes. The anabolic cartilage markers *ACAN* and *FN1* were significantly down-regulated in the *FN1* mutant chondrocytes as compared with wild type, while the catabolic and hypertrophic markers *ADAMTS-5*, *ALPL*, and *RUNX2* were significantly up-regulated in the *FN1* homozygous group (**Figure 6** and **Table 2**). These data indicate that the mutant chondrocytes were in a more OA disease state, where the effect was stronger in the homozygous mutant group. To investigate the downstream effects of the fibronectin mutation on the fibronectin-binding chondrocyte cell surface integrin receptors, we investigated the gene expression levels of *ITGA3, ITGB1,* and *ITGA5*. Integrin α5β1 is the main fibronectin-binding integrin, while α3β1 and αVβ1 can also bind fibronectin [36, 37]. *ITGA3* and *ITGB1* were significantly up-regulated in *FN1* homozygous chondrocytes (**Figure 6**). Notably, *ITGA5* was down-regulated in the heterozygous group, while its expression was not changed in the homozygous group.

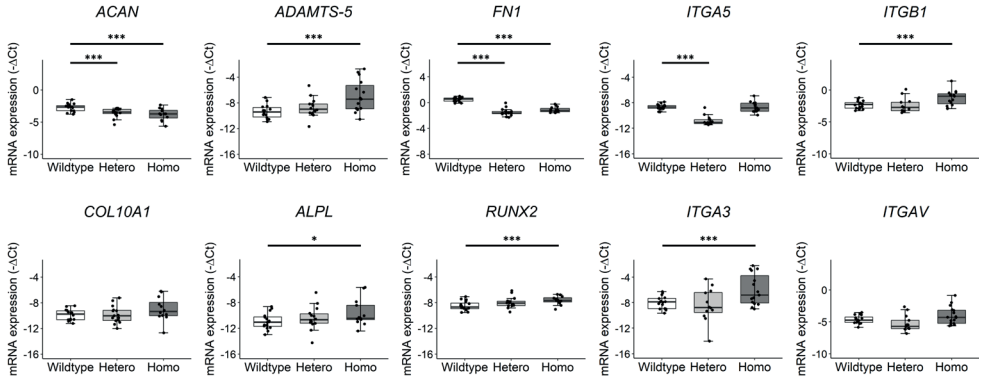

Figure 6 | *FN1* mutation results in aberrant chondrocyte gene expression. Box plots of –ΔCt values of *ACAN*, *ADAMTS-5*, *FN1*, *ITGA5*, *ITGB1*, *COL10A1*, *ALPL*, *RUNX2*, *ITGA3*, *ITGAV* in wild-type, C518F *FN1* heterozygous (Hetero) and homozygous (Homo) chondrogenic pellets. –ΔCt values shown were corrected for *COL1A1* and *COL2A1* expression levels to correct for the difference in efficiency of chondrogenic differentiation between genotypes. The box plots represent 25th, 50th and 75th percentiles, and whiskers extend to 1.5 times the interquartile range. Individual samples are depicted by black dots in each graph. P values were determined by generalized estimation equations, with gene expression levels (-ΔCt) as dependent variable and genotype as factor. * P < 0.05, ** P < 0.01, *** P < 0.005.

Table 2 | Differences in gene expression between C518F *FN1* homozygous and heterozygous human induced chondroprogenitor-derived chondrogenic pellets compared to wild-type after 5 weeks of chondrogenesis.

	Hetero vs Wt*				Homo vs Wt*			
Gene	**FC**	**Beta**	**SE**	**P value**	**FC**	**Beta**	**SE**	**P value**
ACAN	0.57	-0.81	0.23	4.52×10^{-4}	0.57	-1.1	0.24	2.62×10^{-4}
ADAMTS-5	1.55	0.63	0.48	1.93×10^{-1}	5.14	2.36	0.68	5.45×10^{-4}
ALPL	1.41	0.5	0.56	3.79×10^{-1}	2.45	1.3	0.63	4.03×10^{-2}
COL10A1	1.03	0.05	0.41	9.11×10^{-1}	1.86	0.9	0.56	1.09×10^{-1}
FN1	0.25	-1.98	0.16	1.00×10^{-4}	0.33	-1.59	0.13	1.00×10^{-4}
ITGA3	1.18	-0.41	0.77	5.93×10^{-1}	3.91	1.97	0.65	2.51×10^{-3}
ITGA5	0.23	-2.13	0.23	1.00×10^{-4}	1.01	0.02	0.24	9.34×10^{-1}
ITGAV	0.66	-0.6	0.37	1.03×10^{-1}	1.53	0.61	0.37	1.03×10^{-1}
ITB1	0.92	-0.12	0.33	7.20×10^{-1}	2.09	1.07	0.33	1.11×10^{-3}
RUNX2	1.42	0.5	0.28	6.75×10^{-2}	1.79	0.84	0.26	9.48×10^{-4}

*Fold change (FC), Beta value, standard error (SE), and P value for expression levels (-ΔCt) of 10 genes as determined by generalized estimation equations, with gene expression levels (-ΔCt) as dependent variable and genotype as factor, when comparing *FN1* heterozygous (Hetero) and *FN1* homozygous (Homo) pellets to wild-type (Wt) pellets.

Discussion

In the current study, we identified a heterozygous missense mutation (c1,819 G> T; C518F) in *FN1* that is likely causal to the EO phenotype in an extended EO-OA family (**Figure 1**). By introducing this high-impact mutation in hiPSCs using CRISPR/Cas9 gene editing and using them in an established in vitro organoid cartilage model, we showed that the chondrogenic potential (**Figure 3**) and deposition of neo-cartilage (**Figure 4**) of the *FN1* mutant chondrocytes was decreased. Moreover, we demonstrated that the underlying pathogenic mechanism of the mutation was caused by a decreased binding of fibronectin to the surrounding ECM protein collagen type II (**Figure 5**). As a downstream effect, the formed neo-cartilage was prone to a hypertrophic and procatabolic (OA) state, as reflected by the changed chondrocyte gene expression pattern, particularly of *ADAMTS-5* and *RUNX2* (**Figure 6**). This is further confirmed by the up-regulation of *ITGA3* and *ITGB1*, which is comparable to an OA disease state of chondrocytes [37].

Since fibronectin is an important adhesion protein between ECM and chondrocytes via binding to the cell surface integrins, we advocate that the identified C518F mutation in fibronectin hampers essential interaction between chondrocytes and the ECM; hence, plasticity of chondrocytes to adequately respond to cues from the ECM is decreased. In osteoarthritic joints, it has been shown that fibronectin is degraded proteolytically into fragments (FN-fs), which amplify catabolic processes in articular cartilage [38-41]. These FN-fs have distinct activities due to different binding capacities and thereby lead to changes in communication

between the ECM and the chondrocyte. Therefore, it is tempting to speculate that the phenomenon of changed binding could be directly contributing to the onset of age-related OA in the population.

One of the findings in this study is that the *FN1* mutant hiCPCs compared to wild type had both reduced chondrogenic potential (**Figure 3**). These results are in line with previous findings showing that the presence of fibronectin matrix is essential for mesenchymal stromal cell condensation and chondrogenic differentiation [42, 43]. The results of our study therefore suggest that decreased binding between fibronectin and collagen type II may negatively affect these processes. To elucidate the exact mechanism of during differentiation, longitudinal analysis of the differentiation would have to be performed in future studies.

The less efficient formation of dense, round pellets as a result of the mutation (**Figure 3**), hence variable quantity of neo-cartilage formed in the *FN1* mutant pellets, was a confounding factor in the gene expression data analyses. We observed a lower amount of cartilage-producing cells relative to the total amount of cells in *FN1* mutated pellets compared with wild type, as well as a decrease in the deposition of neo-cartilage (**Figure 4**). As a result, an overall stepwise decrease in cartilage-specific gene expression was observed in the *FN1* mutant pellets. To adjust for the relatively lower amount of cartilage formed in the *FN1* mutant chondrogenic pellets, we used the cartilage-specific markers *COL2A1* and *COL1A1* as reference genes. We chose *COL2A1* and *COL1A1* for their typically high expression in cartilage, as well as their stability in ongoing OA pathophysiology as reflected by a previously published large RNA sequencing dataset of autologous cartilage [26], and that we showed to be specific markers for the neo-cartilage (**Figure 4A**). Although we are confident that the observed significant increase in *ADAMTS-5*, *ALPL*, and *RUNX2* and the significant decrease in *ACAN* and *FN1* expression reflected true biological effects (**Figure 6**), the accuracy of the fold changes provided may be affected. There are different possibilities to overcome this problem in the future. Recently, Adkar *et al.* [20] engineered a knock-in *COL2A1-GFP* reporter system in hiPSCs to purify chondroprogenitors, consequently improving chondrogenic capacity during differentiation. To be able to further investigate the effect of the mutation on chondrogenesis without the decrease in chondrogenic potential, the *COL2A1* reporter system could be used for our *FN1* OA disease model to circumvent this effect. On the other hand, single-cell RNA sequencing could identify the chondroprogenitor subpopulation in the heterogeneous pellets, so that gene expression analysis of only that subpopulation would be possible [31].

Notably, even after correcting for *COL2A1* and *COL1A1* as cartilage specific markers, *FN1* and *ACAN* expression was significantly decreased in *FN1* mutant pellets, likely affecting quality of deposited cartilage matrix. Moreover, *ITGA3* and *ITGB1* were significantly up-regulated in the *FN1* homozygous pellets. Since α3β1 integrin was shown to be up-regulated in OA chondrocytes,

the here observed switch from α5β1 to α3β1 integrins in *FN1* homozygous chondrocytes may reflect an unbeneficial disease state of the *FN1* homozygous chondrocytes [37]. Conversely, *ITGA5* was down-regulated only in the *FN1* heterozygous pellets, which could have been a direct result of the formation of wild type-mutant fibronectin dimers, thereby also potentially being responsible for the decreased *FN1* and *ACAN* expression. Recently, it has been shown that the fibronectin-α5β1 adhesion is essential for tissue regeneration in mice [44]. These data indicate that the mutation results in aberrant chondrocyte gene expression, potentially via a change in integrin subunit expression levels toward a more hypertrophic, catabolic state, possibly due to decreased binding between fibronectin and collagen type II. However, this should be confirmed by more investigative studies on protein level, e.g., by Western blot to quantify protein levels of the integrin subunits.

Previous studies regarding familial, high-impact *FN1* mutations have been associated with glomerulopathy with fibronectin deposits (GDND), which is a hereditary kidney disease with proteinuria, microscopic hematuria, and hypertension, as well as spondylometaphyseal dysplasia with "corner factures" [45, 46]. These mutations were located in multiple heparin-binding domains, which play an essential role in regulating fibronectin assembly into organized fibrils in ECM. When comparing the phenotypes associated to the *FN1* mutations, it is notable that the phenotype in our family is less severe since glomerulopathy results in renal failure and the spine and growth plates are affected in spondylometaphyseal dysplasia, resulting in, amongst others, shortened trunk and scoliotic posture. Apparently, a mutation in the gelatin-binding domain results in a more specific pathology involving only the joints. The previously identified mutations also often involved cysteine residues, confirming that proper folding of fibronectin, e.g., via disulfide bonds, is crucial for the binding of fibronectin to other matrix components. Together, these data highlight the importance of proper binding of fibronectin to collagen in articular cartilage.

Together, by combining exome sequencing and linkage analysis we demonstrated that the identified *FN1* mutation is causal to human primary OA at an age of onset around 20 to 40 years. Moreover, the mutation does not cause severe developmental aberrations; yet, it has sufficient impact on cartilage tissues to allow measurable functional in vitro effects. Furthermore, by precise genetic engineering of a registered hiPSC line without off-target effects (**Supplementary Figure 2**), we established both a hetero- and homozygous isogenic clone with the OA causing *FN1* mutation (**Figure 2**). By subsequently applying an established differentiation protocol able to produce biomimetic human neo-cartilage, we generated multiple reliable biological replicates on how aberrant function of fibronectin in cartilage is causal to OA onset. Hence, we are confident that our approach was able to create reliable data highly translating to the human in vivo situation while contributing to the societal need to reduce animal studies.

In conclusion, our approach highlights the immense potential of combining exome sequencing, hiPSCs, CRISPR/Cas9, and organoid disease modeling to uncover previously unknown underlying disease mechanisms that are readily extrapolated to novel therapeutic avenues in common, complex human genetic diseases. Particularly, we here show that the underlying pathogenic mechanism of the mutation was caused by a decreased binding of fibronectin to the surrounding ECM protein collagen type II. Moreover, as reflected by the changes in chondrocyte gene expression, particularly of *ADAMTS-5* and *RUNX2,* such impaired binding results in the cartilage becoming prone to enter an OA disease state. In addition, we observed a switch in expression levels of the main fibronectin-binding receptor integrin α5β1 to integrin α3β1, reflecting a more OA disease state of the chondrocytes. Together our work merits further exploration of fibronectin as potential target for therapeutic interventions. We advocate that restoring or maintaining proper binding between fibronectin and collagen type II should be the focus of such a quest.

Acknowledgements

We thank all the members of the MolEpi Osteoarthritis group for valuable discussion and feedback. We thank specifically Rodrigo Coutinho de Almeida and Margo Tuerlings for providing the RNA sequencing data of lesioned and preserved OA cartilage and bone. We thank prof. dr. Christine Mummery for the initial help with the hiPSC work and dr. Manuel Gonçalves for the help with the design of the CRISPR/Cas9 components. Data were generated within the scope of the Medical Delta Programs Regenerative Medicine 4D: Generating Complex Tissues With Stem Cells and Printing Technology and improving Mobility with Technology.

Funding:

Dutch Scientific Research council NWO /ZonMW VICI scheme grant nr 91816631/528 (IM)
Dutch Arthritis Society grant nr DAF-16-1-405 & DAF-16-1-406 (IM)
US National Institutes of Health grant nr AG15768 (FG)

References

1. Goldring, S.R. and M.B. Goldring, *Changes in the osteochondral unit during osteoarthritis: structure, function and cartilage-bone crosstalk*. Nat Rev Rheumatol, 2016. **12**(11): p. 632-644.
2. Conaghan, P.G., et al., *Osteoarthritis research priorities: a report from a EULAR ad hoc expert committee*. Ann Rheum Dis, 2014. **73**(8): p. 1442-5.
3. van der Kraan, P.M., et al., *Translation of clinical problems in osteoarthritis into pathophysiological research goals*. RMD Open, 2016. **2**(1): p. e000224.
4. Litwic, A., et al., *Epidemiology and burden of osteoarthritis*. Br Med Bull, 2013. **105**: p. 185-99.

5. Cirulli, E.T. and D.B. Goldstein, *Uncovering the roles of rare variants in common disease through whole-genome sequencing*. Nat Rev Genet, 2010. **11**(6): p. 415-25.
6. Rabbani, B., et al., *Next-generation sequencing: impact of exome sequencing in characterizing Mendelian disorders*. J Hum Genet, 2012. **57**(10): p. 621-32.
7. Goldstein, D.B., et al., *Sequencing studies in human genetics: design and interpretation*. Nat Rev Genet, 2013. **14**(7): p. 460-70.
8. Adkar, S.S., et al., *Genome Engineering for Personalized Arthritis Therapeutics*. Trends Mol Med, 2017. **23**(10): p. 917-931.
9. Takahashi, K., et al., *Induction of pluripotent stem cells from adult human fibroblasts by defined factors*. Cell, 2007. **131**(5): p. 861-72.
10. Meulenbelt, I., et al., *Strong linkage on 2q33.3 to familial early-onset generalized osteoarthritis and a consideration of two positional candidate genes*. Eur J Hum Genet, 2006. **14**(12): p. 1280-7.
11. Ramos, Y.F., et al., *A gain of function mutation in TNFRSF11B encoding osteoprotegerin causes osteoarthritis with chondrocalcinosis*. Ann Rheum Dis, 2015. **74**(9): p. 1756-62.
12. Min, J.L., et al., *Mutation analysis of candidate genes within the 2q33.3 linkage area for familial early-onset generalised osteoarthritis*. Eur J Hum Genet, 2007. **15**(7): p. 791-9.
13. Deelen, J., et al., *Genome-wide association study identifies a single major locus contributing to survival into old age; the APOE locus revisited*. Aging Cell, 2011. **10**(4): p. 686-98.
14. Riyazi, N., et al., *Evidence for familial aggregation of hand, hip, and spine but not knee osteoarthritis in siblings with multiple joint involvement: the GARP study*. Ann Rheum Dis, 2005. **64**(3): p. 438-43.
15. Keurentjes, J.C., et al., *Patients with severe radiographic osteoarthritis have a better prognosis in physical functioning after hip and knee replacement: a cohort-study*. PLoS One, 2013. **8**(4): p. e59500.
16. Ramos, Y.F., et al., *Genes involved in the osteoarthritis process identified through genome wide expression analysis in articular cartilage; the RAAK study*. PLoS One, 2014. **9**(7): p. e103056.
17. Meulenbelt, I., et al., *Meta-analyses of genes modulating intracellular T3 bio-availability reveal a possible role for the DIO3 gene in osteoarthritis susceptibility*. Ann Rheum Dis, 2011. **70**(1): p. 164-7.
18. Dambrot, C., et al., *Polycistronic lentivirus induced pluripotent stem cells from skin biopsies after long term storage, blood outgrowth endothelial cells and cells from milk teeth*. Differentiation, 2013. **85**(3): p. 101-9.
19. Bae, S., J. Park, and J.S. Kim, *Cas-OFFinder: a fast and versatile algorithm that searches for potential off-target sites of Cas9 RNA-guided endonucleases*. Bioinformatics, 2014. **30**(10): p. 1473-5.
20. Adkar, S.S., et al., *Step-Wise Chondrogenesis of Human Induced Pluripotent Stem Cells and Purification Via a Reporter Allele Generated by CRISPR-Cas9 Genome Editing*. Stem Cells, 2019. **37**(1): p. 65-76.
21. Rodriguez Ruiz, A., et al., *Cartilage from human-induced pluripotent stem cells: comparison with neo-cartilage from chondrocytes and bone marrow mesenchymal stromal cells*. Cell Tissue Res, 2021.
22. Farndale, R.W., D.J. Buttle, and A.J. Barrett, *Improved quantitation and discrimination of sulphated glycosaminoglycans by use of dimethylmethylene blue*. Biochim Biophys Acta, 1986. **883**(2): p. 173-7.
23. Bomer, N., et al., *Underlying molecular mechanisms of DIO2 susceptibility in symptomatic osteoarthritis*. Ann Rheum Dis, 2015. **74**(8): p. 1571-9.
24. Faas, F.G., et al., *Virtual nanoscopy: generation of ultra-large high resolution electron microscopy maps*. J Cell Biol, 2012. **198**(3): p. 457-69.
25. Kiezun, A., et al., *Deleterious alleles in the human genome are on average younger than neutral alleles of the same frequency*. PLoS Genet, 2013. **9**(2): p. e1003301.
26. Coutinho de Almeida, R., et al., *RNA sequencing data integration reveals an miRNA interactome of osteoarthritis cartilage*. Ann Rheum Dis, 2019. **78**(2): p. 270-277.
27. Tuerlings, M., et al., *RNA sequencing reveals interacting key determinants of osteoarthritis acting in subchondral bone and articular cartilage*. Arthritis Rheumatol, 2020.
28. Stoffels, J.M., C. Zhao, and W. Baron, *Fibronectin in tissue regeneration: timely disassembly of the scaffold is necessary to complete the build*. Cell Mol Life Sci, 2013. **70**(22): p. 4243-53.

29. Pankov, R. and K.M. Yamada, *Fibronectin at a glance*. J Cell Sci, 2002. **115**(Pt 20): p. 3861-3.
30. Vinod, E., P. Boopalan, and S. Sathishkumar, *Reserve or Resident Progenitors in Cartilage? Comparative Analysis of Chondrocytes versus Chondroprogenitors and Their Role in Cartilage Repair*. Cartilage, 2018. **9**(2): p. 171-182.
31. Dicks, A., et al., *Prospective isolation of chondroprogenitors from human iPSCs based on cell surface markers identified using a CRISPR-Cas9-generated reporter*. Stem Cell Res Ther, 2020. **11**(1): p. 66.
32. Su, X., et al., *CD146 as a new marker for an increased chondroprogenitor cell sub-population in the later stages of osteoarthritis*. J Orthop Res, 2015. **33**(1): p. 84-91.
33. Wang, S., et al., *RaptorX-Property: a web server for protein structure property prediction*. Nucleic Acids Res, 2016. **44**(W1): p. W430-5.
34. Hadler, N.M., et al., *Ultrastructure of a hyaluronic acid matrix*. Proc Natl Acad Sci U S A, 1982. **79**(2): p. 307-9.
35. Thyberg, J., *Electron microscopy of cartilage proteoglycans*. Histochem J, 1977. **9**(3): p. 259-66.
36. Loeser, R.F., *Integrins and chondrocyte-matrix interactions in articular cartilage*. Matrix Biol, 2014. **39**: p. 11-6.
37. Loeser, R.F., C.S. Carlson, and M.P. McGee, *Expression of beta 1 integrins by cultured articular chondrocytes and in osteoarthritic cartilage*. Exp Cell Res, 1995. **217**(2): p. 248-57.
38. Zack, M.D., et al., *Identification of fibronectin neoepitopes present in human osteoarthritic cartilage*. Arthritis Rheum, 2006. **54**(9): p. 2912-22.
39. Homandberg, G.A., R. Meyers, and D.L. Xie, *Fibronectin fragments cause chondrolysis of bovine articular cartilage slices in culture*. J Biol Chem, 1992. **267**(6): p. 3597-604.
40. Reed, K.S.M., et al., *Transcriptional response of human articular chondrocytes treated with fibronectin fragments: an in vitro model of the osteoarthritis phenotype*. Osteoarthritis Cartilage, 2020.
41. Homandberg, G.A., R. Meyers, and J.M. Williams, *Intraarticular injection of fibronectin fragments causes severe depletion of cartilage proteoglycans in vivo*. J Rheumatol, 1993. **20**(8): p. 1378-82.
42. Singh, P. and J.E. Schwarzbauer, *Fibronectin matrix assembly is essential for cell condensation during chondrogenesis*. J Cell Sci, 2014. **127**(Pt 20): p. 4420-8.
43. Singh, P. and J.E. Schwarzbauer, *Fibronectin and stem cell differentiation - lessons from chondrogenesis*. J Cell Sci, 2012. **125**(Pt 16): p. 3703-12.
44. Almonte-Becerril, M., et al., *Genetic abrogation of the fibronectin-alpha5beta1 integrin interaction in articular cartilage aggravates osteoarthritis in mice*. PLoS One, 2018. **13**(6): p. e0198559.
45. Lee, C.S., et al., *Mutations in Fibronectin Cause a Subtype of Spondylometaphyseal Dysplasia with "Corner Fractures"*. Am J Hum Genet, 2017. **101**(5): p. 815-823.
46. Castelletti, F., et al., *Mutations in FN1 cause glomerulopathy with fibronectin deposits*. Proc Natl Acad Sci U S A, 2008. **105**(7): p. 2538-43.

Supplementary Table 1 | Radiographic and clinical abnormalities in members of a family with early-onset osteoarthritis.

Patient #	Sex	Age of onset	DIJ	PIJ	MCJ	CMC	Elbow	Shoulder	Hip	Knee	Foot	Ankle	CS	LS	Confirmed ROA
3	F	45	+	+		OA				OA		OA			Yes
4	F	-	-	-	-	-	-	-	-	-	-	-	-	-	-
6	M	40	+	+						OA	+	+			Yes
7	M	-	-	-	-	-	-	-	-	-	-	-	-	-	-
8	F	50	+	+						+			+		No
9	F	40	+	+						+	+	+			No
10	M	43	OA	OA	OA		+	+		+		OA			Yes
11	M	40	+	+							+	OA	OA	OA	Yes
12	F	39	OA	OA	OA				OA	+	+	+			Yes
13	M	-	-	-	-	-	-	-	-	-	-	-	-	-	-
14	F	28	OA	OA	OA					OA		OA		OA	Yes
15*	F	30	+	+	+					+					No
16	F	-	-	-	-	-	-	-	-	-	-	-	-	-	-
17	F	23	H	B		OA		-	-	OA	-	-			Yes

F = female, M = male, OA = Radiographic osteoarthritis, Kellgren Lawrence grade 2 or higher in one or both joints, + = joint complaints, - = no x-ray available or no joint complaints, H = Heberden nodes, B = Bouchard nodes, DIJ = distal interphalangeal joints, PIJ = proximal interphalangeal joints, MCJ = metacarpophalangeal joint, CMC = carpometacarpal joint, CS = cervical spine, LS = lumbar spine, confirmed ROA = confirmed radiological OA.
* patient 15 is a monozygotic twin with patient 14, since there was no confirmed ROA, patient 15 was removed from the linkage analysis

Supplementary Table 2 | Variant prioritization scheme applied after exome sequencing.

	Subject 10
Total number of variants detected	73,407
Exonic including 5'UTR and 3'UTR	20,062
Missense, nonsense, readthrough, frame error, splice site	7,907
Novel	1,032
Missense damaging, nonsense, readthrough, frame error, splice site	122

Supplementary Table 3 | Genotyping of the detected *FN1* variant in familial osteoarthritis family members.

Patient #	Status	FN1 - C518F
3	Affected	C A
4	Unaffected	C C
6	Affected	C A
7	Unaffected	C C
8	Diagnostic uncertain	C C
9	Diagnostic uncertain	C C
10	Affected	C A
11	Affected	C A
12	Affected	C A
13	Unaffected	C C
14	Affected	C A
16	Unaffected	C C
17	Affected	C A

Supplementary Table 4 | Design of CRISPR/Cas9 system. In the single-strand oligonucleotide template the introduced silent mutation to give a HincII restriction site is depicted in italic font and the restriction site is shown in grey, the wanted *FN1* mutation is depicted in bold font, and the mutated PAM site is depicted underlined.

guide RNA	5'- AACAAUGCACUGAUCUGUUU-3'
single-strand oligonucleotide template	5'-CAG CAT GTG CCC CTC TTC ATG ACG CTT GTG GAA TGT GTC GTT CAC ATT GTA AGT GAT GTC *G*TC AAC AAT G**A**A CTG ATC TGT TTA CGA AAC AGG TGG GTG AGT GAG AAA CTT TTT AAA GTT CCA TTG ATG AAA GAA AAA AGG-3'

Supplementary Table 5 | Primer sequences to measure mRNA expression levels, amplify region of interest around *FN1* mutation (exon 11), and amplify off-target region.

Region of interest	Forward primer (5' --> 3')	Reverse primer (5' --> 3')
ACAN	AGAGACTCACACAGTCGAAACAGC	CTATGTTACAGTGCTCGCCAGTG
ADAMTS-5	GTGGTGAAGGTGGTGGTGCT	CTCATGGTCATCTCCCAGCTG
ALPL	CAAAGGCTTCTTCTTGCTGGTG	CCTGCTTGGCTTTTCCTTCA
COL1A1	GTGCTAAAGGTGCCAATGGT	ACCAGGTTCACCGCTGTTAC
COL2A1	CTACCCCAATCCAGCAAACGT	AGGTGATGTTCTGGGAGCCTT
COL10A1	GGCAACAGCATTATGACCCA	TGAGATCGATGATGGCACTCC
FN1	CCGACCAGAAGTTTGGGTTC	CACGACCATTCCCAACACAC
GAPDH	TGCCATGTAGACCCCTTGAAG	ATGGTACATGACAAGGTGCGG
ITGA5	GTCGGGGGCTTCAACTTAGAC	AGCACACTGACCCCGTCTG
ITGA3	TGCCTACAACTGGAAAGGAAAC	CTGCCTACCTGCATCGTGTA
ITGAV	TCTCTCGGGACTCCTGCTAC	AAGAAACATCCGGGAAGACGC
ITGB1	AGCGAAGGCATCCCTGAAAG	AATGTCTACCAACACGCCCT
MCAM	GGAAGTCACCGTCCCTGTTT	ATGCTGAAGTGTGGTGGAGG
PDGRFβ	GGACATACCCCCGCAAAGAA	CTCTCCGTCACATTGCAGGT
SDHA	TGGGAACAAGAGGGCATCTG	GCCTACCACCACTGCATCAA
RUNX2	CTGTGGTTACTGTCATGGCG	AGGTAGCTACTTGGGGAGGA
FN1 (exon 11)	TGGCTTCTCACAGGAAAGTGT	CCAGACGACTACCAATATCGAG
gRNA off-target	AGTGAAGGAGATGTGGCTGC	AAGAGCAACGGGGTGAACAA

Supplementary Table 6 | List of damaging missense variants in an affected family member of an early-onset OA family after our applied prioritization scheme. Base change is base of the sense strand of the DNA.

Chrom.	Gene Name	Ensembl ID	Base change	Base position	Codon change	Substitution
1	CPSF3L	ENSG00000127054	A/G	1250997	GTA-GcA	V46A
1	RBMXL1	ENSG00000213516	T/G	89448812	GAT-GcT	D233A
1	ITGA10	ENSG00000143127	C/T	145530939	ACG-AtG	T224M
1	NBPF14	ENSG00000122497	C/A	148004625	GTG-tTG	V897L
1	ADAMTSL4	ENSG00000143382	G/A	150531177	GAC-aAC	D871N
1	LINGO4	ENSG00000213171	G/A	151774330	TCC-TtC	S284F
1	SELE	ENSG00000007908	A/T	169697065	GTG-GaG	V428E
1	C1orf129	ENSG00000117501	G/A	170961360	GTG-aTG	V362M
1	HEATR1	ENSG00000119285	A/G	236722383	GTG-GcG	V1527A
1	ZP4	ENSG00000116996	G/A	238050846	ACC-AtC	T190I
2	GPR113	ENSG00000173567	G/A	26534245	GCG-GtG	A784V
2	MOBKL1B	ENSG00000114978	A/G	74399827	TCT-cCT	S23P
2	DNAH6	ENSG00000115423	A/T	84899498	ATG-tTG	M2168L
2	MMADHC	ENSG00000168288	C/T	150436081	GGT-GaT	G79D
2	ALS2	ENSG00000003393	A/C	202590176	TAT-gAT	Y1084D
2	FN1	ENSG00000115414	C/A	216285518	TGC-TtC	C518F
2	ABCB6	ENSG00000115657	G/C	220075737	CGT-gGT	R688G
3	DNAH12	ENSG00000174844	G/C	57401178	GCA-GgA	A1924G
3	NEK11	ENSG00000114670	G/C	130748679	GTC-cTC	V43L
3	PAK2	ENSG00000180370	G/C	196529902	CAG-CAc	Q101H
4	MFSD10	ENSG00000109736	A/C	2935381	TAT-gAT	Y61D
4	MAN2B2	ENSG00000013288	T/A	6596307	ATG-AaG	M302K
4	TMPRSS11	ENSG00000198092	G/A	68930465	TCT-TtT	S318F
4	FAM13A	ENSG00000138640	A/C	89660254	GTG-GgG	V830G
4	GPRIN3	ENSG00000185477	T/G	90170862	ACC-cCC	T134P
4	NHEDC1	ENSG00000164037	A/C	103832643	CTG-CgG	L294R
4	SEC24D	ENSG00000150961	G/A	119678880	CCA-tCA	P473S
4	FRG1	ENSG00000109536	C/T	190874234	CCT-tCT	P91S
4	FRG1	ENSG00000109536	C/A	190878563	GCT-GaT	A148D
5	CDC20B	ENSG00000164287	G/A	54423155	CGG-tGG	R307W
5	PPIC	ENSG00000168938	C/T	122361517	GGC-aGC	G158S
5	LECT2	ENSG00000145826	C/T	135287013	GGA-GaA	G63E
5	PCDHB8	ENSG00000120322	G/A	140558064	GGG-GaG	G150E
5	ZNF354C	ENSG00000177932	A/G	178507004	TAT-TgT	Y524C
6	ZNF318	ENSG00000171467	G/A	43307399	CCA-CtA	P1446L
7	SDK1	ENSG00000146555	G/A	4002375	GGA-aGA	G441R
7	HBP1	ENSG00000105856	G/C	106836335	CGC-CcC	R375P
7	SLC26A3	ENSG00000091138	T/G	107427841	AAA-AAc	K283N
7	CFTR	ENSG00000001626	C/T	117188750	TCT-TtT	S422F
7	OR9A2	ENSG00000179468	A/C	142723621	GTT-GgT	V200G
7	GALNT11	ENSG00000178234	T/C	151810377	GTA-GcA	V376A
7	MLL3	ENSG00000055609	A/G	151919751	TGT-cGT	C1114R
8	PABPC1	ENSG00000070756	G/A	101721812	CGC-tGC	R374C
8	PABPC1	ENSG00000070756	T/C	101721817	GAA-GgA	E372G
8	PABPC1	ENSG00000070756	C/A	101721839	GTA-tTA	V365L
8	FER1L6	ENSG00000214814	C/T	124989741	CGG-tGG	R319W
8	PLEC	ENSG00000178209	A/G	145003292	CTG-CcG	L1217P
8	ZNF251	ENSG00000198169	T/C	145979657	GAG-GgG	E28G
9	EXOSC3	ENSG00000107371	G/C	37782053	CGA-gGA	R186G

Chrom.	Gene Name	Ensembl ID	Base change	Base position	Codon change	Substitution
9	NOTCH1	ENSG00000148400	T/C	139390627	AGC-gGC	S2522G
10	IL15RA	ENSG00000134470	G/A	6008296	ACG-AtG	T32M
10	ARMC3	ENSG00000165309	A/G	23250814	GAT-GgT	D180G
10	PLAU	ENSG00000122861	C/T	75673437	CGG-tGG	R165W
10	LIPM	ENSG00000173239	C/A	90579993	ACT-AaT	T336N
10	TM9SF3	ENSG00000077147	C/A	98292928	TGT-TtT	C402F
10	CPXM2	ENSG00000121898	C/G	125521390	GGA-GcA	G592A
11	OR51S1	ENSG00000176922	C/A	4870162	GCC-tCC	A93S
11	DNHD1	ENSG00000179532	C/T	6585157	CGC-tGC	R3363C
11	OLFML1	ENSG00000183801	C/T	7509386	ACG-AtG	T53M
11	SAA4	ENSG00000148965	T/A	18254071	GAC-GtC	D34V
11	LGR4	ENSG00000205213	A/T	27390683	TTT-TTa	F529L
11	BTBD18	ENSG00000233436	A/G	57513573	TTC-cTC	F58L
11	ATM	ENSG00000149311	T/C	108214007	ATT-AcT	I2776T
11	CRYAB	ENSG00000109846	C/A	111781098	GTG-tTG	V93L
12	FOXM1	ENSG00000111206	T/C	2967952	AAT-AgT	N753S
12	PZP	ENSG00000126838	G/A	9307415	CGC-tGC	R1191C
12	SLC11A2	ENSG00000110911	G/C	51384724	CGG-gGG	R477G
12	NUAK1	ENSG00000074590	C/A	106460782	CGC-CtC	R595L
13	CCNA1	ENSG00000133101	G/A	37014187	CGA-CaA	R322Q
13	KIAA1704	ENSG00000133114	G/T	45589633	GGT-tGT	G33C
14	HEATR5A	ENSG00000129493	G/A	31762650	TCT-TtT	S1995F
14	RALGAPA1	ENSG00000174373	A/G	36103797	CTC-CcC	L1534P
14	MTHFD1	ENSG00000100714	A/C	64884707	ACC-cCC	T194P
14	PLEKHG3	ENSG00000126822	C/T	65198849	CAC-tAC	H332Y
14	DIO2	ENSG00000211448	T/C	80669078	GAG-GgG	E259G
14	DDX24	ENSG00000089737	A/C	94521529	GTC-GgC	V664G
14	CDC42BPB	ENSG00000198752	C/G	103410810	GCT-cCT	A1276P
14	PACS2	ENSG00000179364	A/G	105821407	AGG-gGG	R106G
15	HERC2	ENSG00000128731	G/A	28483865	CGC-tGC	R1211C
15	ARHGAP11	ENSG00000198826	G/C	32921855	GAT-cAT	D333H
15	RYR3	ENSG00000198838	G/T	34152828	GAC-tAC	D4774Y
15	KIF23	ENSG00000137807	C/A	69709740	CCA-aCA	P34T
15	AKAP13	ENSG00000170776	G/T	86270411	GTC-tTC	V2317F
16	RGS11	ENSG00000076344	T/C	323545	CAG-CgG	Q152R
16	TBL3	ENSG00000183751	A/G	2024410	AGC-gGC	S75G
16	TSC2	ENSG00000103197	T/C	2130361	CTG-CcG	L1198P
16	ACSM5	ENSG00000183549	C/T	20429546	CGG-tGG	R124W
16	ABCC11	ENSG00000121270	C/T	48218359	GTG-aTG	V1084M
16	SALL1	ENSG00000103449	C/T	51171034	GTC-aTC	V1322I
16	GLG1	ENSG00000090863	T/C	74514287	GAC-GgC	D560G
16	KIAA1609	ENSG00000140950	A/G	84531559	TTC-TcC	F45S
17	FAM57A	ENSG00000167695	G/A	644611	CGG-CaG	R160Q
17	ALOX12B	ENSG00000179477	T/C	7977033	TAT-TgT	Y566C
17	CCDC144A	ENSG00000170160	G/A	16664922	GAA-aAA	E1186K
17	LGALS9C	ENSG00000171916	G/A	18397608	CGC-CaC	R333H
17	TRAF4	ENSG00000076604	C/T	27076578	CGG-tGG	R466W
17	SLFN11	ENSG00000172716	A/G	33680081	ATT-AcT	I667T
17	CDC27	ENSG00000004897	A/C	45216160	GTT-GgT	V550G

Chrom.	Gene Name	Ensembl ID	Base change	Base position	Codon change	Substitution
17	CDC27	ENSG00000004897	G/A	45216182	CTT-tTT	L543F
17	ABCC3	ENSG00000108846	G/A	48762223	GGG-aGG	G1423R
17	PYCR1	ENSG00000183010	G/A	79893008	CGG-tGG	R112W
18	DSG1	ENSG00000134760	C/T	28934644	CCT-tCT	P829S
19	MATK	ENSG00000007264	C/G	3779073	GGC-cGC	G372R
19	SH2D3A	ENSG00000125731	T/C	6755228	AGG-gGG	R199G
19	XAB2	ENSG00000076924	A/G	7685456	TGC-cGC	C691R
19	HAUS8	ENSG00000131351	C/T	17170885	GGA-aGA	G83R
19	ISYNA1	ENSG00000105655	C/T	18546943	GCG-aCG	A90T
19	ZNF98	ENSG00000197360	T/C	22574988	TAC-TgC	Y350C
19	MEGF8	ENSG00000105429	T/C	42855627	TGG-cGG	W968R
19	ZNF285	ENSG00000062370	C/T	44890654	GAG-aAG	E585K
19	ZNF285	ENSG00000062370	G/C	44891010	GCG-GgG	A466G
19	PPP1R13L	ENSG00000104881	G/A	45885802	CCG-tCG	P385S
19	DMWD	ENSG00000185800	T/C	46290117	AAG-gAG	K213E
19	ZNF845	ENSG00000213799	T/C	53856761	TGT-cGT	C861R
19	ZNF813	ENSG00000198346	T/C	53995143	TGT-cGT	C553R
19	ZNF543	ENSG00000178229	C/T	57839675	CCT-CtT	P282L
20	XKR7	ENSG00000101321	C/G	30556211	GCG-GgG	A78G
21	TSPEAR	ENSG00000175894	T/C	45941975	AGT-gGT	S453G
22	SOX10	ENSG00000100146	T/C	38374107	GAG-GgG	E155G
22	L3MBTL2	ENSG00000100395	G/C	41615519	GCC-cCC	A233P
22	SCUBE1	ENSG00000159307	C/T	43604155	CGC-CaC	R886H
X	MAGEA6	ENSG00000197172	A/C	151870145	ATT-cTT	I279L

Chrom. = chromosome.

Supplementary Figures

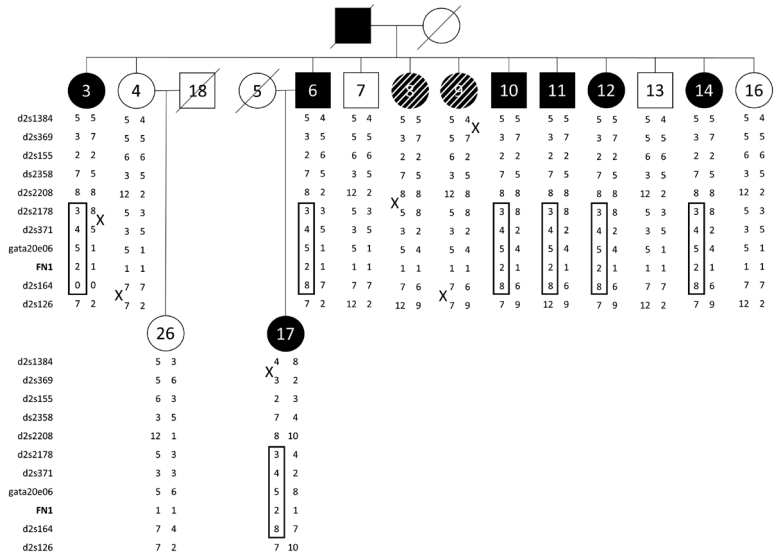

Supplementary Figure 1 | Pedigree of investigated early-onset osteoarthritis family. Co-segregating haplotypes among affected individuals are depicted as squared boxes and recombination as crosses. Individual 10 was used for exome sequencing. Circles represent females, squares represent males. Closed and open shapes represent affected and healthy individuals, respectively; striped shapes represent uncertain phenotypes.

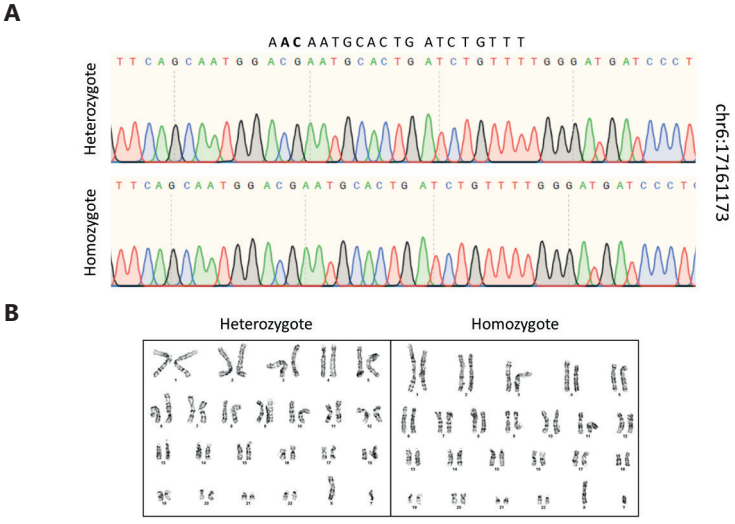

Supplementary Figure 2 | Quality control *FN1* mutant iPSC clones. (**A**) Sanger sequencing results of in silico predicted off-target site at chr6:17161173 allowing 2 mismatches for the heterozygote and homozygote FN1 clone. Sequence of guide RNA is depicted above, where mismatches are depicted in bold. (**B**) Karyotypes of isogenic iPSC lines heterozygous and homozygous for FN1 mutation, showing absence of chromosomal abnormalities.

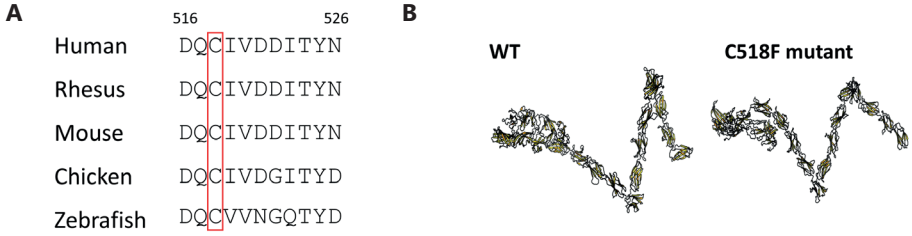

Supplementary Figure 3 | Investigation of C518F fibronectin mutation. (**A**) Alignment of the amino acid sequence around C518 of *FN1*, where the identified mutation is located. Mutated residue is outlined in red. (**B**) Structure prediction of wild-type (WT) and C518F mutant fibronectin by RaptorX of the 1,980 N-terminal amino acid residues.

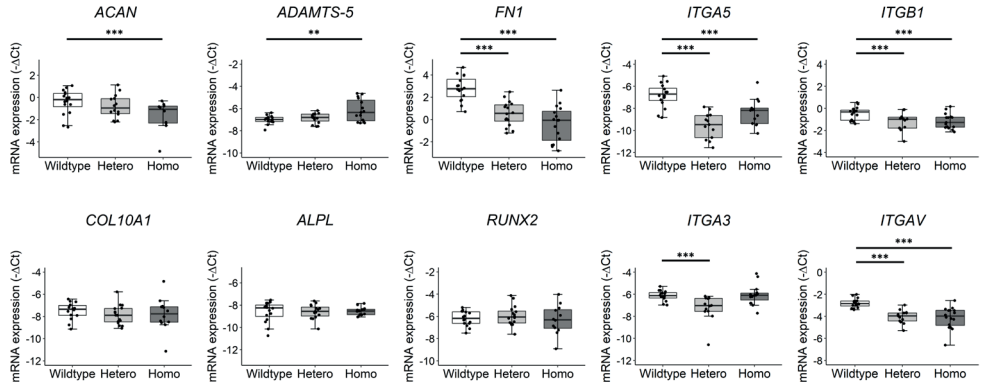

Supplementary Figure 4 | Box plots of –ΔCt values of *ACAN*, *ADAMTS-5*, *FN1*, *ITGA5*, *ITGB1*, *COL10A1*, *ALPL*, *RUNX2*, *ITGA3*, *ITGAV* in wild-type, C518F *FN1* hetero- (Hetero) and homozygous (Homo) chondrogenic pellets. –ΔCt values shown were corrected for *GAPDH* and *SDHA* expression levels. The box plots represent 25th, 50th and 75th percentiles, and whiskers extend to 1.5 times the interquartile range. Individual samples are depicted by black dots in each graph. P values were determined by generalized estimation equations, with gene expression levels (-ΔCt) as dependent variable and genotype as factor. * $P < 0.05$, ** $P < 0.01$, *** $P < 0.005$.